ADVANCED FUNCTIONAL MATERIALS
www.afm-journal.de

# 3D Printed Template-Assisted Casting of Biocompatible Polyvinyl Alcohol-Based Soft Microswimmers with Tunable Stability

*Roger Sanchis-Gual, Hao Ye, Towa Ueno, Fabian C. Landers, Lukas Hertle, Siyu Deng, Andrea Veciana, Yanming Xia, Carlos Franco, Hongsoo Choi, Josep Puigmartí-Luis, Bradley J. Nelson, Xiang-Zhong Chen,* and Salvador Pané**

**The past decade has seen an upsurge in the development of small-scale magnetic robots for various biomedical applications. However, many of the reported designs comprise components with biocompatibility concerns. Strategies for fabricating biocompatible and degradable microrobots are required. In this study, polyvinyl alcohol (PVA)-based magnetic hydrogel microrobots with different morphologies and tunable stability are developed by combining a 3D printed template-assisted casting with a salting-out process. 3D sacrificial micromolds are prepared via direct laser writing to shape PVA-magnetic nanoparticle composite hydrogel microrobots with high architectural complexity. By adjusting the PVA composition and salting-out parameters, the hydrogel dissolubility can be customized. Due to their high mobility, tunable stability, and high biocompatibility, these PVA-based magnetic microrobots are suitable platforms for targeted drug and cell delivery.**

## 1. Introduction

Significant efforts have been made in the past two decades to develop magnetic micro- and nanorobots for various biomedical applications, such as targeted drug delivery, microsurgery, sensing, and diagnosis.[1–6] The broad interest in these devices arises from the fact that they can realize minimally invasive procedures by accessing hard-to-reach regions in the human body thanks to both their small dimensions and untethered motion capabilities. Research endeavors in micro- and nanorobots have focused on multiple factors including their design, fabrication, locomotion, and functionalization.[7–11] However, a major hurdle that hinders the translation of these devices to practical clinical applications is the biocompatibility aspect of their building blocks, as many small-scale magnetic robots comprise materials that can trigger cytotoxic effects. In the past 5 years, efforts have been made to manufacture these devices with biocompatible materials. Advances have been made with the integration of soft materials, which are not only more adaptable to the mechanical and physicochemical characteristics of cells and tissues, but they are also less cytotoxic than other families of materials, such as metals and alloys. However, for the miniaturization of soft materials, the use of some chemical moieties is necessary for their processability at micro- and nanoscales. For example, several 3D printed soft microrobots rely on the use of acrylate groups,[12,13] which can potentially induce inflammatory, cytocidal, or carcinogenic responses upon degradation, and are usually difficult to excrete

R. Sanchis-Gual, H. Ye, T. Ueno, F. C. Landers, L. Hertle, S. Deng, A. Veciana, C. Franco, B. J. Nelson, X.-Z. Chen, S. Pané
Multi-Scale Robotics Lab
Institute of Robotics and Intelligent Systems
ETH Zürich
Tannenstrasse 3, Zürich CH-8092, Switzerland
E-mail: chenxian@ethz.ch; vidalp@ethz.ch

Y. Xia
Department of Mechanical & Electrical Engineering
Xiamen University
Xiamen 361005, China

The ORCID identification number(s) for the author(s) of this article can be found under https://doi.org/10.1002/adfm.202212952.



**DOI: 10.1002/adfm.202212952**

H. Choi
Department of Robotics and Mechatronics Engineering
DGIST-ETH Microrobot Research Center
Daegu-Gyeongbuk Institute of Science & Technology (DGIST)
333 Techno jungang-daero, Hyeonpung-eup, Dalseong-gun, Daegu 42988, Republic of Korea

J. Puigmartí-Luis
Departament de Ciència dels Materials i Química Física
Institut de Química Teòrica i Computacional
University of Barcelona (UB)
Barcelona 08028, Spain

J. Puigmartí-Luis
ICREA
Institució Catalana de Reserca i Estudis Avançats
Pg. Lluís Companys 23, Barcelona 08010, Spain

from the human body.[14–16] Therefore, the development of soft microrobots composed of materials that display optimal tissue contact, reduced immune responses, and the ability to dissolve or degrade to nontoxic and metabolizable products once their tasks have been completed, is essential.[17,18]

Polyvinyl alcohol (PVA) is a water-soluble polymer with impressive features, including good biocompatibility characteristics, biodegradability, customizable chemical structures (e.g., molecular weight, degree of hydrolysis, derivatization), among others.[19–21] Furthermore, this polymer can be safely used in the human body as it can be biodegraded by oxidation and hydrolysis into mono/di-ketones and carbonyl structures,[22] which are easily metabolized. For this reason, PVA has been approved by the Food and Drug Administration for pharmaceutical coatings and vasculature embolization agents, making it a promising candidate for degradable microrobots. The molecular structures of PVA can be easily tuned, which allows its properties, such as mechanical properties and dissolubility, to be easily customized.[23–25] For example, a simple salting-out process can transform dissolved PVA into hydrogels that remain stable in water by crystallizing/aggregating the polymer chains and introducing physical crosslinking points. This is caused by the expulsion of water molecules between the polymer chains and the hydrogen bonds formed between the hydroxyl groups.[26–28] Interestingly, salted-out PVA hydrogels retain good biocompatibility features.[23] However, the realization of PVA-based microswimmers remains challenging because the salting-out process of PVA is difficult to integrate with laser-based direct 3D forming techniques. For this reason, very few PVA-based microrobots have been reported so far. Kim et al. designed spherical PVA microrobots for drug delivery using an emulsion-based fabrication.[29] However, this method is not suitable for the fabrication of more complex architectures, such as helices and grids, which are usually required for locomotion or other functionalities. To date, PVA microrobots with complex shapes have only been achieved in large dimensions (larger than 1 mm in size) and with complicated setups.[30,31]

Here, we developed 3D magnetic PVA microrobots with different shapes and enhanced stability by combining the salting-out process with an indirect 3D molding method.[32] In this indirect molding technique, direct laser writing was first employed to produce 3D sacrificial templates with high architectural complexity and resolution. These templates can be used to cast polymers that cannot be directly 3D-printed at the microscale.[32,33] This method enables the preparation of PVA hydrogel-based biocompatible and degradable soft microrobots with the desired morphology. Additionally, by tuning the PVA compositions and salting out parameters, we were able to customize the hydrogel dissolubility. Our approach, which can be extended to several polymer formulations, can be used to construct soft microrobots with enhanced biocompatibility and tunable stability for therapeutic application.

## 2. Results and Discussion

### 2.1. Microrobot Fabrication

The indirect 3D printing method, depicted in **Figure 1**a, was used to prepare 3D magnetic PVA microstructures. In the first step, the substrate was coated with a layer of positive photoresist. Following direct laser writing and development, cavities with various well-defined shapes were obtained. The cavity structures were created in such a way that for each structure, several openings were left on the top surface of the positive photoresist. In this way, after developing, a PVA solution containing magnetic $Fe_3O_4$ nanoparticles (MNPs) could be infiltrated into the cavities (Figure S1, Supporting Information). Note that the MNPs are coated with a biocompatible and biodegradable polymer (polyvinylpyrrolidone (PVP))[34] to prevent particle agglomeration in the solution. These MNPs can be biodegraded within intracellular lysosomes due to the combined effect of acidic pH, digestive enzymes and iron chelators, resulting in the transfer of iron to ferritin proteins.[35,36] Although these MNPs were chosen because of their high biocompatibility,[37] others such as FePd[38] or FePt[39] could potentially be used. Next, the salting-out process was carried out by immersing the PVA composite in a highly concentrated salt solution (e.g., sodium citrate). Ions in the salt solution make PVA chains crystallize/aggregate through self-coalescence, causing phase separation. Salted-out hydrogels are more robust, and this process is critical for improving the stability of PVA in aqueous solutions while retaining their high biocompatibility.[23] Indeed, the resulting non-salted-out microrobots instantly deformed and dissolved in aqueous solution, even when they had a defined shape before immersion in water (Figure S2, Supporting Information). Finally, the magnetic PVA microrobots were released by dissolving the photoresist with acetone. Figure 1b shows complex structures with different designs and shapes, demonstrating the versatility of the current method.

For use as microrobotic components, the PVA structures must be stable in aqueous solutions. Figure 1c shows a representative PVA microstructure that is stable in water, its shape is well maintained, and it is only slightly swollen when compared to the microstructure in acetone. Figure 1d,e shows magnified Scanning Electron Microscopy (SEM) images of a part of a helical microstructure before and after hydration. The diameter of the filament increased from 17 to 25 μm due to swelling. The surface of the microrobot is not fractured and is quite homogeneous after hydration. It should be noted that the released PVA structures were transferred to water by progressively replacing acetone with water (Figure S3, Supporting Information). This solvent exchange step must be done gradually to control the swelling of the PVA microstructures as abrupt hydration can lead to undesired structural changes. Once PVA microstructures have swollen to their final shape after a controlled immersion in water, they become stable. They even exhibit high reversibility between the drying and hydration cycles. Figure S4 (Supporting Information) shows a PVA cage that was cyclically hydrated and dried three times without being distorted. This excellent property can facilitate their storage and manipulation at a later stage.

### 2.2. PVA Stability

As mentioned above, the properties of PVA hydrogel, especially the dissolubility, can be easily modified by adjusting the synthetic parameters. In this way, once these composites are

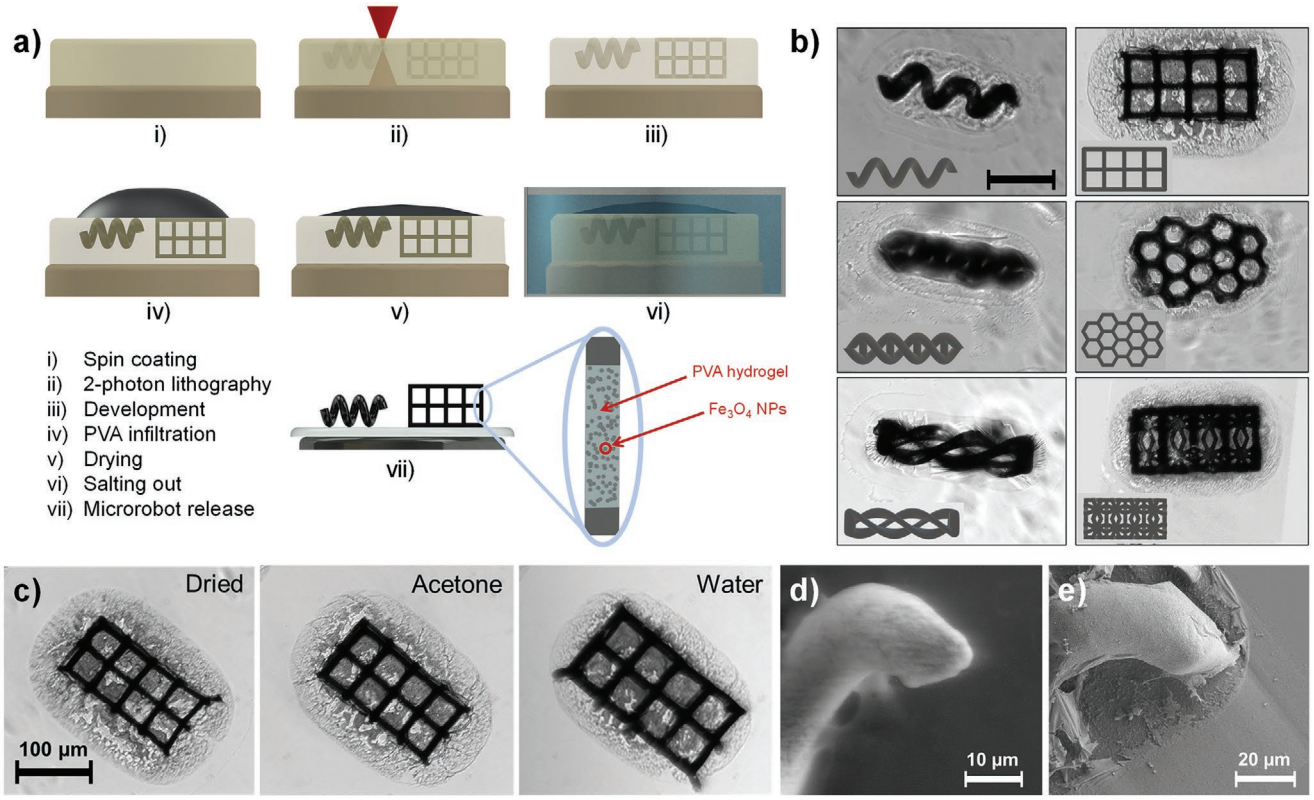


**Figure 1.** a) Fabrication steps of salted-out PVA magnetic microrobots: i) Positive tone photoresist spin-coated onto a glass substrate, ii,iii) direct laser writing and developing of the 3D template, iv) infiltration of PVA in the template, v) drying, vi) salting out, vii) PVA microrobot release. b) Optical images of different magnetic salted-out PVA microrobot structures immersed in acetone. The scale bar corresponds to 100 µm. The insets correspond to the designs used for printing the microstructures. c) Optical images of a magnetic PVA cage microstructure in air, acetone, and water. d) Environmental-SEM image of a dried magnetic PVA helix. e) Cryo-SEM image of a hydrated magnetic PVA helix.

dissolved in the human body, they will be biodegraded by PVA-oxidases and $\beta$-diketone hydrolases.[22,40] This feature allows the lifetime of the microrobots to be customized depending on their application scenario. To this end, the influence of several parameters on the PVA hydrogel's stability, including the molecular weight (Mw), concentration, degree of hydrolysis, salt concentration, and salting-out duration, has been analyzed (**Figure 2**). PVA MNPs composite disks were fabricated and salted-out, and the weight variation of these disks was recorded at different time points after soaking in an aqueous solution (see Experimental Section for further details) to reveal the dissolution kinetics. Four different aqueous solutions (DI water, phosphate-buffered saline (PBS), artificial cerebrospinal fluid (aCSF), and simulated body fluid (SBF)) were chosen to evaluate the PVA hydrogels' dissolubility in different biological environments.

Figure 2a shows the influence of different molecular weights on the stability of the PVA hydrogels. PVAs with a high degree of hydrolysis (>99%) and three different molecular weights (31, 68, and 130 kDa) have been tested. For the PVA with the smallest molecular weight, the hydrogel disks dissolved almost immediately after immersion in the solution, which was most probably caused by a limited degree of entanglement between the polymer chains. Stable hydrogels can form when the molecular weight is over 68 kDa. The hydrogels' weight peaked after ≈1 h due to swelling, then decreased slightly over time in the next 3 days. Although a molecular weight of 130 kDa can form stable hydrogels, the viscosity is so high that the PVA solution cannot effectively infiltrate into the 3D printed cavities to shape microrobots. Therefore, we selected 68 kDa to perform the rest of the study. The concentration of the PVA solution also influences the final hydrogel. Hydrogels made with 5 wt.% PVA can be quickly dissolved. Stable hydrogels can only be produced when the concentration is greater than 10 wt.%. All of the stable hydrogels started losing weight after 1 h because of the slow disentanglement of the polymer chains at the physical crosslink points.[41] However, hydrogels made with higher concentrations (15 wt.%) could absorb more water in all cases. As a result of the high swelling of the 15 wt.% PVA, we chose 10 wt.% as the concentration for the remainder of the study. Note that by varying the molecular weight or the concentration, the hydrogel can either disappear quickly or remain stable for a long time (more than 3 days). Thus, these parameters are not appropriate for adjusting the dissolution of the hydrogel.

In contrast to molecular weight and concentration, the degree of hydrolysis is a key parameter that enables fine control over the dissolubility of the hydrogel (Figure 2c; Figure S5, Supporting Information). The degree of hydrolysis corresponds to the ratio between the vinyl alcohol unit and the vinyl acetate unit on the polymer chain. The higher degree of hydrolysis corresponds to a higher amount of −OH groups on the polymer chains and a stronger and more stable salted-out hydrogel.

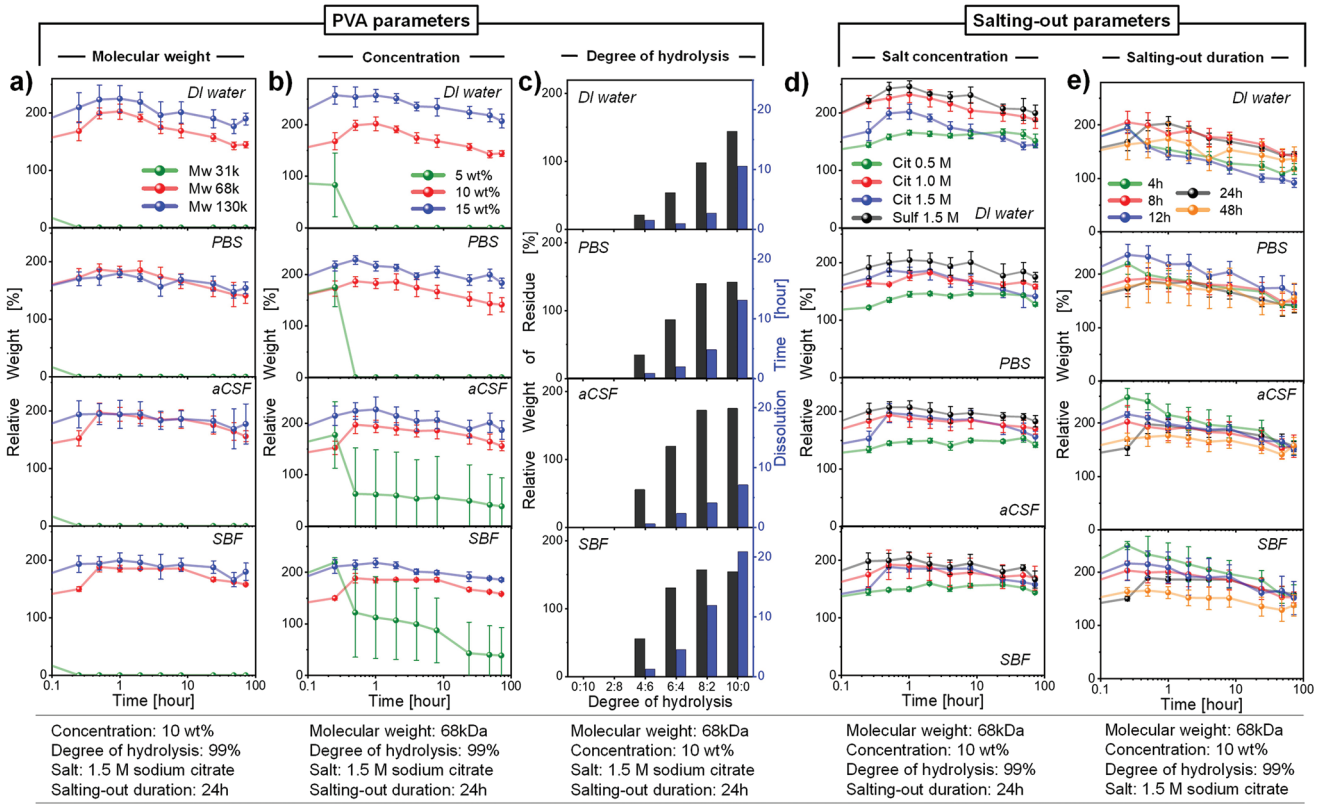


**Figure 2.** Stability over time of the salted-out PVA hydrogel (mixed with MNPs) disks in different aqueous solutions as a function of the following synthetic parameters: a) molecular weight, b) concentration, c) degree of hydrolysis, d) salt concentration, and e) salting-out duration. Graphs in the third column show the final mass after 3 days in solution (black bars) and the time at which the total dissolved hydrogel mass is halved (blue bars). 100% of the relative weight corresponds to the initial mass of the disks before being soaked in the aqueous solution.

We thus tuned the dissolubility of the hydrogels by varying the mixing ratio of PVAs with two different degrees of hydrolysis (99% and 87%, respectively). In the case of the highest degree (99%:87% in a ratio of 10:0), the hydrogel remains stable even after 3 days. When changing the ratio, the hydrogels start to dissolve after 10–50 h (8:2), 1–2 h (6:4), 15–30 min (4:6), or a few minutes (2:8 and 0:10) (detailed data can be found in Figure S5, Supporting Information). In order to clearly present the trend, we extracted the residual weights after 72 h and the dissolving times (see the experimental section for the definition and calculation), and the results are shown in Figure 2c. We can see that the higher the portion of the PVA with 99% degree of hydrolysis in the mixture, the slower the hydrogel dissolves, and the higher residual is left after 72 h. This trend can be observed in all four aqueous solutions. Note that in the simulated physiological fluids, such as aCSF and SBF, both the residual weights and the time constants are higher than those in DI water, indicating that salt concentration can slow down the dissolution of the hydrogels.

The parameters of the salting-out process also influence the dissolution process of the hydrogel. The more concentrated the salt solution used for salting-out, the more difficult it is to dissolve the hydrogel, as has been reported earlier.[23,26,42] However, in general, the dissolution trend did not show significant differences. For hydrogels made with 10 wt.% PVA with a 99% degree of hydrolysis, the weight change over 3 days was minor, indicating a high stability. We also tried using different salts, and we found that sodium citrate produces less swelling compared to sodium sulfate, and the tested concentrations did not show important mass differences over time. In the same manner, the duration of the salting-out process did not make a significant difference.

The effect of the concentration of MNPs was also investigated. First, the water stability of magnetic PVA disks with varying PVA:MNPs ratios was analyzed (Figure S6, Supporting Information). As can be observed, when the ratio is <3:7, the resulting structures are not enough stable and lose weight rather than gaining because of hydration. Therefore, ratios higher than 3:7 are required to form stable structures. Taking this into account, the mass variation over time of stable magnetic PVA disks with different MNPs concentrations was examined (Figure S7, Supporting Information). The resulting trends do not differ significantly, indicating that, for stable structures (PVA:MNPs ratios higher than 3:7), the concentration of magnetic NPs has no noticeable impact on their dissolution.

Last but not least, we investigated the dissolution process of PVA structures at the microscale to determine how many of these microstructures could potentially be used after a certain time (**Figure 3**; Figure S8–S10, Supporting Information). Thin stripes of 13 µm wide, 13 µm high, and 220 µm long were prepared using a stamping method,[43] as one such microstructure has a similar volume to a micro helical structure with a filament

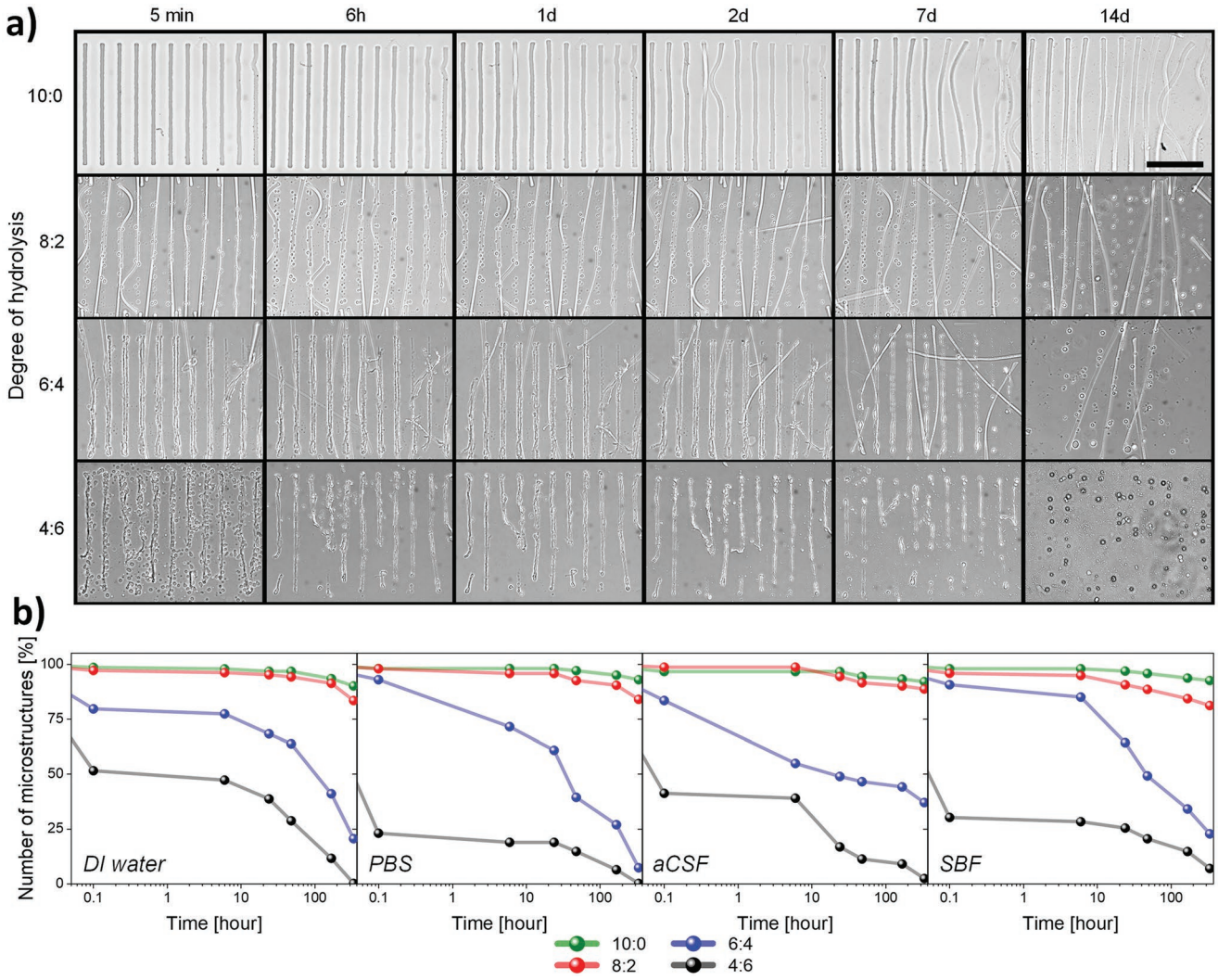


**Figure 3.** a) Stability of the salted-out PVA hydrogel (without MNPs) microstructures in DI water as a function of the degree of hydrolysis over 2 weeks. MNPs were not added to facilitate the visual evaluation of PVA dissolution. The scale bar corresponds to 100 µm. b) Evolution of the number of microstructures in different aqueous solutions over time. Broken and almost dissolved microstructures have not been counted.

diameter of 15 µm. In this way, it was possible to quickly test a large number of PVA microstructures (>100) to obtain statistically relevant information. Figure 3a shows representative images of the microstructures in DI water taken at different time intervals. Here, we fixed all other parameters including molecular weight (Mw 66 kDa), concentration (10 wt.%), salt solution (sodium citrate 1.5 M), and salting-out duration (24 h). The only varying parameter was the ratio of the two PVAs with different degrees of hydrolysis. As can be observed, the stability of the PVA hydrogel with the highest degree of hydrolysis is very high. There was no sign of dissolution after 2 weeks, even though some structures swelled and changed their shapes. This type of hydrogel could be used for long-term applications (e.g., embolization) inside the human body thanks to its high stability. As previously observed, the dissolution time accelerates when the mixing ratio decreases. For example, in the case of an 8:2 ratio, almost no broken structures were found, but many were bent or became thinner. These effects were more evident when a 6:4 ratio was used, where the PVAs microstructures were highly degraded after 1 week, and it was possible to observe some hydrogel residues on the surface. We hypothesize that the solvent has more difficulty diffusing into the polymer network (and dissolving it) when the hydrogel is on the substrate surface. These two ratios could be employed for microrobots that are used for a few days. When using a 4:6 ratio, the hydrogel is degraded after 1 day and, consequently, more than 50% of the structures are broken or dissolved (Figure 3b). Thus, a microrobot made of this PVA could be applied for several hours before becoming nonoperational. If the ratio is decreased further (2:8 and 0:10 ratios), then the structures are completely degraded when introduced to water. By tuning the mixing ratio, we can easily obtain microrobots with customized dissolution times to meet the requirements of different drug delivery applications.[44]

### 2.3. Biocompatibility Study

The biocompatibility features of the microrobots are key for their biomedical application. **Figure 4**a demonstrates the

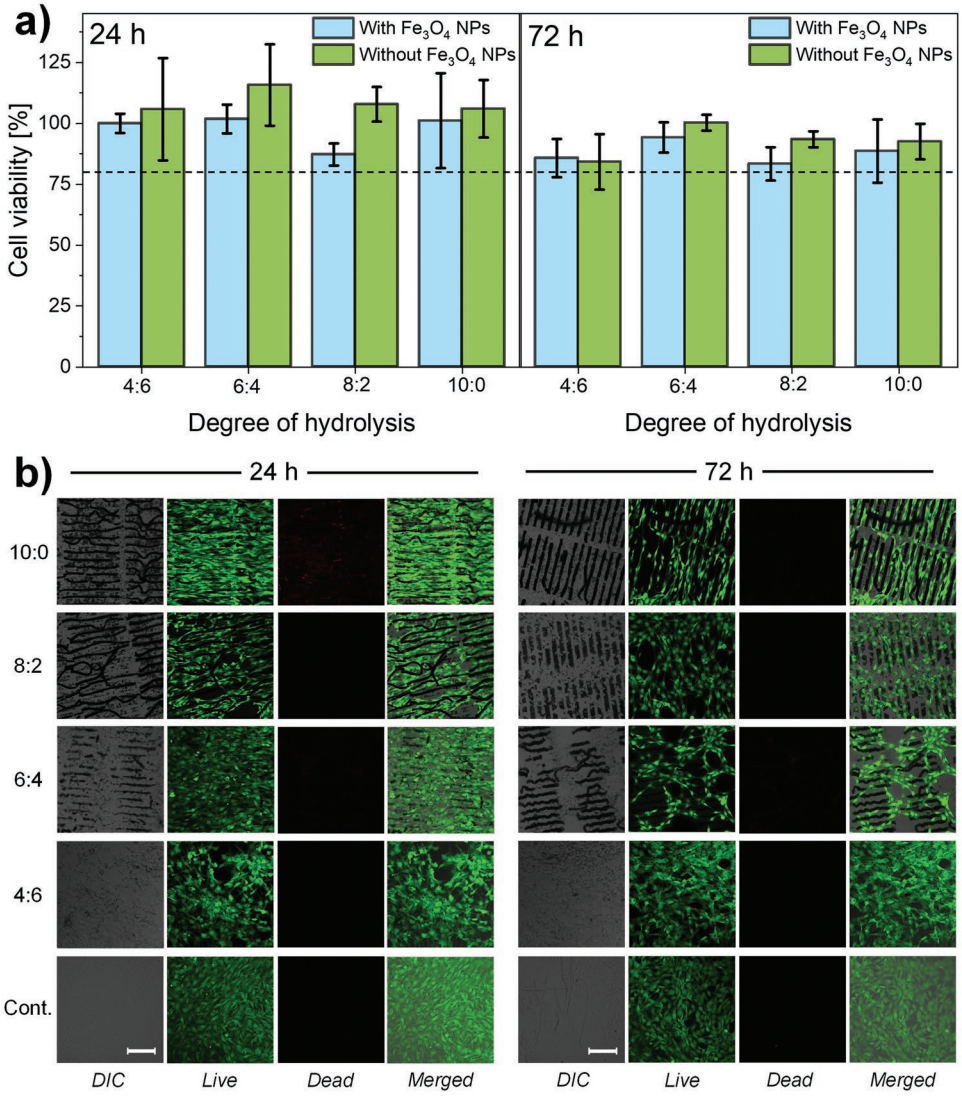


**Figure 4.** a) MTT assays with NIH/3T3 cells. In vitro cytotoxicity after 24 (left) and 72 (right) h of incubation. b) Live/dead cell viability assays of NIH/3T3 cells cultured on salted-out magnetic PVA hydrogels after 24 (left) and 72 (right) h of incubation. The quantification results are shown in Figure S11 (Supporting Information). The scale bar corresponds to 100 µm. Relative cell viability was calculated by ImageJ ($n = 3$).

biocompatibility of the PVA hydrogels with NIH/3T3 cells. Cell viability after 24 and 72 h of incubation in the presence of PVA hydrogel disks is over 80%, regardless of the degree of hydrolysis. Although the addition of MNPs slightly reduces cell viability, all the samples are considered biocompatible because the cell viability is kept above the cytotoxic limit (80%; ISO 10993–5:2009). Live/dead cell viability assays were also performed on the patterned magnetic PVA hydrogels to further confirm the biocompatibility (Figure 4b). In all cases, the cells grew perfectly in the presence of the salted-out hydrogels with almost no dead cells (Figure 4b; Figure S11, Supporting Information). Furthermore, the dissolution of the PVA (4:6 sample) did not cause adverse effects. Thus, the magnetic PVA hydrogels prepared with the salting-out method display biocompatibility characteristics and show great potential for use in biomedical applications. Indeed, the good biocompatibility of the hydrogel allowed us to load cells onto a magnetic PVA grid shaped microstructure for targeted cell delivery (Figure S12, Supporting Information). We can see that the cells can readily interact with and proliferate inside the structure. This interaction is strong enough to cause structural distortions. Therefore, these microswimmers have the potential to deliver cells for cell therapy and could be used as mobile implantable scaffolds.[45,46]

### 2.4. Microrobot Actuation

The PVA hydrogel microrobots can be easily manipulated thanks to the presence of MNPs (Figure S13, Supporting Information, VSM) homogeneously distributed in the whole structure (Figure S14, Supporting Information). Here we demonstrate the targeted motion of the microrobots with different locomotion modes. **Figure 5**a (also Video S1, Supporting Information) shows that a helical microrobot can be propelled by

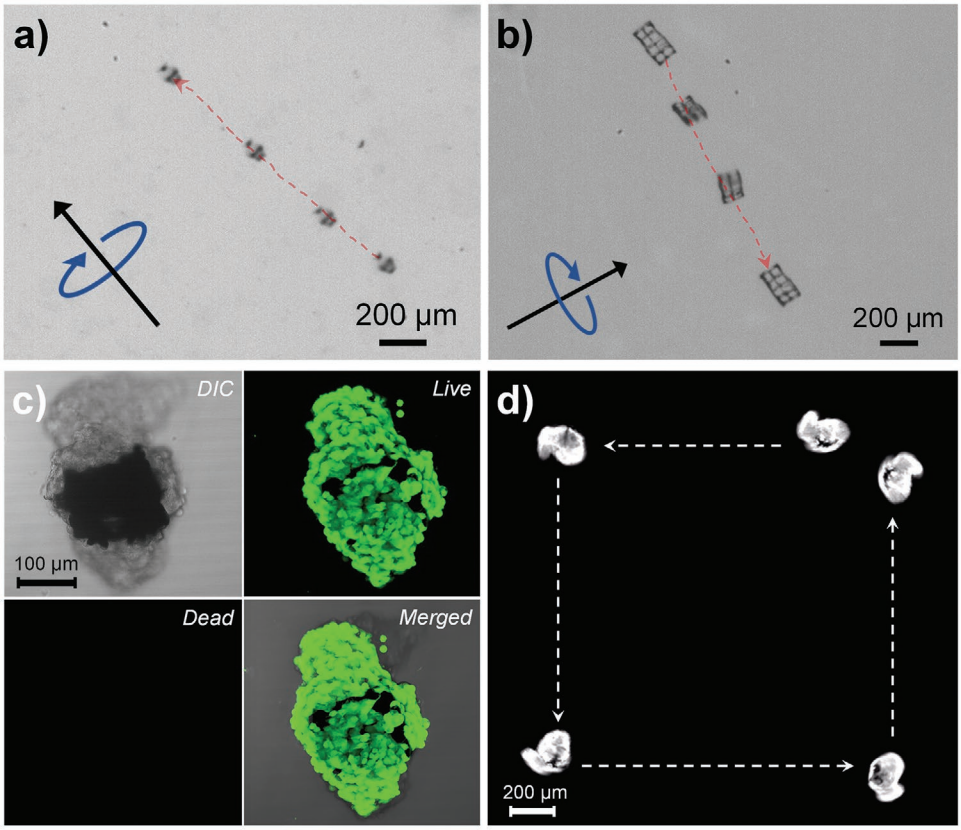


**Figure 5.** Time-lapse images showing the trajectory of a) a helical PVA hydrogel microrobot and b) a PVA hydrogel grid microrobot under magnetic manipulation in DI water. The axis of rotation is indicated by a black arrow and the rotating magnetic field is represented by a blue arrow. c) Live/dead cell viability assays of SH-SY5Y cells cultured on a salted-out magnetic PVA microrobot after 72 h of incubation. d) Fluorescent time-lapse images showing the trajectory of a PVA hydrogel grid microrobot wrapped in SH-SY5Y cells under magnetic manipulation in PBS solution.

corkscrew motion under a rotating magnetic field, which is an efficient and well-known propulsion strategy at the low Reynolds number regime.[32,47] In this regard, the combination of a rotating magnetic field of 20 mT with a frequency of 30 Hz and a gravity-compensating magnetic gradient of 550 mT $m^{-1}$ was used to actuate the microrobot to swim along various trajectories in DI water inside a glass petri dish. The microrobot showed an excellent magnetic response with a high forward velocity (65.5 µm $s^{-1}$) and a relatively low sideways drift velocity (11.1 µm $s^{-1}$). The observed drift during the actuation was mostly caused by the friction between the microrobot and the surface substrate. As another example, a grip shaped microrobot was also successfully manipulated with a rotating magnetic field (15 mT, 2 Hz, gravity compensating magnetic field of 300 mT $m^{-1}$) (Figure 5b; Video S2, Supporting Information). In this case, the structure was able to move forward along a trajectory with little drift by rolling on the surface.

Considering the high mobility, high biocompatibility features, and excellent interaction of these microstructures with cells, we explored their application as cell delivery systems. A magnetic PVA grid microrobot was incubated with SH-SY5Y cells for 72 h to form a cell spheroid-microrobot complex (Figure 5c). The cells were checked by means of the live/dead assay, and it can be observed that almost all the cells are alive (green color channel). We then conducted manipulation experiments using green fluorescence as a tracer (Figure 5d; Video S3, Supporting Information). Despite the presence of the cells, the microrobot exhibits a strong magnetic response. The cell-laden microrobot can be actuated with a small rotating magnetic field (10 mT, 1 Hz) and a gravity-compensating field gradient of 300 mT $m^{-1}$ to follow a pre-defined trajectory. These results demonstrate that these biocompatible PVA microstructures could be applied as a safe platform for cell delivery.

## 3. Conclusion

In this study, we prepared PVA-based hydrogel soft microrobots with different morphologies and tunable stability. We elaborated a protocol that relies on a 3D mold casting approach and a salting-out process to overcome the instability of PVA microstructures in aqueous solutions. The dissolubility of the PVA hydrogels can be tuned by changing the synthetic conditions, where the degree of hydrolysis of the PVA was the most critical parameter. Moreover, the magnetic PVA hydrogels prepared using the salting-out method exhibit extremely low levels of cytotoxic effects. By using small magnetic fields, the different PVA structures can be easily and precisely manipulated. We also demonstrated that these biocompatible PVA microstructures could be a superior platform for live cell transportation.

The high mobility, tunable stability, and biocompatibility enable these degradable magnetic microrobots to be applied safely for drug delivery and even cell delivery.

## 4. Experimental Section

*Chemicals and Materials*: Polyvinyl alcohol (98–99% hydrolyzed, molecular weight: 31 000–50 000; 99+% hydrolyzed, molecular weight: 89 000–98 000; 86.7–88.7% hydrolyzed, molecular weight: ≈67 000; 99+% hydrolyzed, molecular weight: 130 000), sodium citrate tribasic dihydrate, sodium sulfate, and phosphate buffered saline were purchased from Sigma–Aldrich. Polydimethylpolysiloxane (PDMS: SYLGARD 184) and its hardener were acquired from Dow Europe GmbH (Wiesbaden, Germany). Iron oxide nanoparticles (purity: 99.5%, 15–20 nm, 20 wt.%) were obtained from US Research Nanomaterials, Inc. (Houston, USA). All other chemical reagents were obtained from Sigma–Aldrich and were used without any further purification.

*PVA Solution Preparation*: The 5, 10, and 15 wt.% PVA solutions were prepared by dissolving PVA powder. Each solution was mixed using a magnetic stirrer rotated at 180 rpm and heated at 90 °C. After PVA dissolved completely, the solution was sonicated for 30 min at 60 °C in order to degas it. The solutions with different degrees of hydrolysis were prepared by mixing PVA 99+% and 86.7-88.7% hydrolyzed at certain ratios (10:0, 8:2, 6:4, 4:6, 2:8, and 0:10). These PVAs were mixed using a magnetic stirrer rotated at 600 rpm for 2 h.

*Magnetic PVA Solution Preparation*: An equal amount of PVA and MNPs solutions were mixed with a vortex for 15 min and tip-sonicated at 50% duty ratio and 50% power for 2.5 min in order to fully distribute the MNPs throughout the solution.

*PVA Microrobot Fabrication*: Photoresist templates were prepared on a 30 mm diameter glass coverslip using Nanoscribe (photonic Professional GT). Initially, a positive tone photoresist (AZ IPS-6090) was spin-coated by accelerating at 300 rpm $s^{-1}$ and rotating at 1000 rpm for 17 s, resulting in a photoresist thickness of ≈79–83 µm. This was followed by a baking step where the coated coverslip was heated from room temperature up to 125 °C and kept at 125 °C for 5 min. Next, a drop of immersion oil was applied to the center, and the exposure was started from the oil-photoresist interface using a femtosecond laser of 780 nm and 80 MHz, and a 63× objective. After exposure, the sample was washed with DI water and baked at 110 °C for 1 min. The photoresist was then developed in AZ 726 MIF for 20 min. Afterward, the sample was rinsed with DI water several times and dried. Next, 40 µL PVA-MNP dispersion was dropped on the templates, and then the sample was put in a vacuum for 5 min so that the PVA-MNP dispersion could be infiltrated into the template. After drying, the sample was then salted-out by immersing it in a 1.5 M sodium citrate solution for 24 h, removed from the solution, rinsed with DI water, and left to dry.

*Microrobot Release*: Prior to the release, the photoresist outside the microrobot area was detached and removed using a blade. Acetone was then added to dissolve the remaining photoresist around the microrobots in the presence of a magnet on the bottom of the sample to keep them at the position. The previous acetone was then replaced by new acetone to remove the dissolved photoresist. Afterward, DI water was gradually added to replace the acetone. The remaining acetone was left to evaporate completely, and then DI water was replaced with simulated physiological fluids.

*Morphological Characterization*: Optical images were taken using an Olympus IX81 and a Hirox KH-1300 optical microscope. Environmental SEM images were taken using a Quanta 200F operating at 20 kV, 6.1 mm of working distance, and a pressure of 1000 Pa. Environmental SEM images were taken using an FEI Quanta 200 F microscope operating at 1000 Pa, 20 kV and a working distance of 6.0 mm. For cryo-SEM images, PVA microrobots were hydrated by adding 10 µl of double distilled water. After blotting the residual liquid, the wet structures on the coverslip were manually plunged and frozen in a mix of liquid ethane and propane. The frozen specimens were then transferred and mounted under liquid nitrogen on the cryo-holder and finally transferred under liquid nitrogen into a precooled (–130 °C) freeze-fracturing system BAF 060 (Bal-Tec/Leica, AT) at $3 \times 10^{-6}$ mbar. Freeze-etching (partial freeze-drying) was done at –100 °C for 1 min at a vacuum higher than $1 \times 10^{-6}$ mbar. Afterward, unidirectional tungsten deposition at an elevation angle of 45° to a thickness of 3 nm was followed by 3 nm at 90°. Transfer to the precooled cryo-SEM was done under high vacuum ($<5 \times 10^{-6}$ mbar) with a cold air-lock shuttle VCT010 (Bal-Tec/Leica, AT). Cryo-SEM was performed in a field emission SEM Leo Gemini 1530 (Carl Zeiss, DE) equipped with a cold stage to maintain the specimen temperature at–120 °C (VCT Cryostage, Bal-Tec/Leica, AT). Inlens-SE- and Everhart-Thornley SE-signals at an acceleration voltage of 2 kV were used for image acquisition. SEM images were taken using a Zeiss Ultra 55, operating at 5 kV, 30 aperture and a working distance of 10 mm. EDX images were acquired an OXFORD instruments EDX detector operating at 20 kV and 60 aperture.

*Characterization of Magnetic Properties*: Magnetic hysteresis loops of PVA microrobots in the template were recorded at room temperature with a vibrating sample magnetometer (VSM EZ9, Microsense). The field was scanned from –2T to 2T. Subsequent data correction was performed by removing the contribution of the sample holder and the empty structure substrate.

*PVA Dissolution at the Macroscale*: Five hundred thirty microliters of PVA-MNP dispersion were poured into the chambers of a 24-well plate, with a diameter of ≈15 mm, and allowed to dry completely by natural evaporation. Afterward, 3 mL of salt solution was poured onto the dried sheets to salt them out. The salting-out process lasted from 4 to 48 h, depending on the experiment. The degradation of salted-out PVA hydrogel at the macroscale was evaluated by weighing the PVA sheets soaked in DI water, PBS, aCSF, and SBF aqueous solutions at different times. Each sample was soaked into 3 mL of one of the four aqueous solutions. To weigh the samples, liquid on its surface was removed by putting them between two sheets of filter paper and adding finger pressure several times until there was no visible leakage on the filter paper. The samples were then returned to the previous solution. All the samples were weighed 1) before being soaked, 2) after 15 min, 3) after 30 min, 4) after 1 h, 5) after 2 h, 6) after 4 h, 7) after 8 h, 8) after 1 day, 9) after 2 days, and 10) after 3 days. Figure 2c values were estimated by adjusting Figure S5 (Supporting Information) data to the following equation: $y = y_o + Ae^{-x/b}$, where $y_o$ corresponds to the residual weight. The dissolution time corresponds to the value of the fit curve at which the total dissolved hydrogel mass had been halved.

*PVA Dissolution at the Microscale*: PVA patterns were prepared following a polydimethylpolysiloxane (PDMS) stamping method.[43] PDMS and its hardener were mixed at the weight ratio of 10 to 1. The mixture was vacuumed for 30 min to degas and poured onto the patterned wafer in a plastic tray. The mixture in the tray was heated at 80 °C for 90 min. After curing, the PDMS stamps were peeled from the patterned wafer. To fabricate PVA patterns, 20 µL of a PVA solution was dropped onto a glass slide. Then, a PDMS stamp was put on the solution with its patterned side facing the glass slide. A coverslip was then put on the PDMS stamp, and 25 g of weight was put on the coverslip to press the stamp. After the PVA solution dried, the whole glass slide/PVA/stamp/coverslip stack was salted-out with 1.5 M sodium citrate solution for 24 h. The PVA micropattern degradation was evaluated by observing the PVA patterns soaked in DI water, PBS, aCSF, and SBF aqueous solutions over time. All the samples were directly observed microscopically 1) after 5 min, 2) after 6 h, 3) after 1 day, 4) after 2 days, 5) after 7 days and 6) after 14 days.

*Cell Culturing*: Mouse embryo fibroblasts (NIH/3T3) were grown under Dulbecco's Modified Essential Medium (DMEM, 31 966 021, Thermo Fisher Scientific, Gibco). Human neuroblastoma cells (SH-SY5Y) were cultured in Minimum Essential Medium (MEM, 41 090 028, Thermo Fisher Scientific, Gibco). All cultured cells were supplied by the American Type Collection (ATCC) and all the mediums were enriched with 10% FBS, streptomycin (100 µg $mL^{-1}$), as well as penicillin (100 units/mL). The cells were cultured under 5% $CO_2$ at 37 °C. For the SH-SY5Y spheroid with PVA hydrogel mixture preparation,

cells were first resuspended in 5 mL of medium, and a stock of $1 \times 10^4$ cells $mL^{-1}$ was obtained after the cells were counted (Watson, 17 176 206). The suspensions (200 µL amounts) were then seeded into ultra-low attachment spheroid microplate (Corning, 4515, ≈2000 cells/spheroid) and incubated with PVA hydrogel for 72 h to generate the cell-PVA hydrogel spheroid.

*Cell Viability Tests*: Cell viability tests were conducted with NIH/3T3 cells. PVA hydrogel samples (disks or micropatterns, with or without magnetic nanoparticles) were sterilized under UV light for 2.5 h, immersed in 10% penicillin–streptomycin and Amphotericin B solution (Sigma Aldrich), washed thoroughly with PBS, and transferred into 48-well plates for cell incubation. NIH/3T3 cells were seeded at a density of $3 \times 10^4$ cells/well for 24 h MTT assays and $1.5 \times 10^4$ cells/well for 72 h MTT assays. After incubating for 24 or 72 h, the MTT assay (3 mg $mL^{-1}$) was employed to determine the cell viability. The Varioskan Flash multimode microreader was employed to quantify the absorbance of the samples at 570 nm (reference 630 nm) and the average value from the triplicate wells was calculated.

*Live/Dead Assay*: For the live/dead assay, the NIH/3T3 cells or cell-PVA hydrogel spheroid were incubated with live/dead working solution for 15 min (Invitrogen, Cat: R37601) at room temperature. The cells were then imaged by the confocal microscope (LSM 880 Airyscan, Zeiss) and quantified by ImageJ.

*Immunofluorescence Staining*: The PVA hydrogel samples were first sterilized under UV light, immersed in 10% penicillin-streptomycin and Amphotericin B solution (Sigma Aldrich), and washed thoroughly with PBS. The samples were then set in 35 mm confocal dishes and incubated overnight with fetal bovine serum (Gibco, Cat: 10270106). Thereafter, samples were incubated with the SH-SY5Y cells for 24 h, fixed with 4% PFA, and incubated for 10 min at room temperature. 0.5% of Triton X-100 was then added, and samples were permeabilized for 30 min at room temperature. Blocking of the samples was performed with 2% BSA for 30 min, and then incubated at 4 °C with primary antibodies against βIII-tubulin (Sigma Aldrich, T2200) overnight. Secondary antibody FITC Goat anti-rabbit IgG (Sigma Aldrich, AP132F) was added to the samples and incubated for 1 h, followed by washing and nuclear staining. Images of samples were then obtained using a confocal microscope (LSM 880 Airyscan Zeiss).

*Microrobot Manipulation*: The MiniMag, which was an electromagnetic system for 5-DOF wireless micromanipulation, was utilized for the swimming tests. Magnetic PVA microrobots composed of a molecular weight of 68 kDa, 10 wt.% concentration, 1:1 PVA:MNPs ratio, 10:0 degree of hydrolysis, and salted-out in 1.5 M sodium citrate solution for 24 h were tested. The swimming tests were carried out in DI water or PBS solution by applying a rotating magnetic field in combination with a gravity-compensating magnetic field gradient. An Olympus IX81 fluorescence microscope was used to record the cell transportation experiment.

*Statistical Analysis*: Each data point in the PVA dissolution and cell viability experiments was measured at least three times. The data were presented as mean ± SD.

## Supporting Information

Supporting Information is available from the Wiley Online Library or from the author.

## Acknowledgements

R.S.-G. and H.Y. contributed equally to this work. This work was financed by the ERC Consolidator Grant HINBOTs (No. 771565), the ERC Advanced Grant SOMBOTs (No. 743217), FETPROACT-EIC-05-2019 ANGIE (No. 952152), by the National Research Foundation of Korea (No. 2021M3F7A1082275, No. 2017K1A1A2013237), and the Swiss National Science Foundation (Project No. 192012, 190451). The authors would like to thank the Scientific Center for Optical and Electron Microscopy (ScopeM), and the FIRST laboratory at ETH for their technical support. R.S.-G. thanks the Spanish Ministry of Universities and the European Union for a "Margarita Salas" postdoctoral fellowship (Next Generation EU).

Open access funding provided by Eidgenossische Technische Hochschule Zurich.

## Conflict of Interest

The authors declare no conflict of interest.

## Data Availability Statement

The data that support the findings of this study are available from the corresponding author upon reasonable request.

## Keywords

3D printing, biocompatibility, hydrogels, microrobots, salting out

Received: November 8, 2022
Revised: January 18, 2023
Published online: March 14, 2023

[1] M. Sitti, H. Ceylan, W. Hu, J. Giltinan, M. Turan, S. Yim, E. Diller, *Proc. IEEE* **2015**, *103*, 205.
[2] K. E. Peyer, L. Zhang, B. J. Nelson, *Nanoscale* **2013**, *5*, 1259.
[3] M. Koleoso, X. Feng, Y. Xue, Q. Li, T. Munshi, X. Chen, *Mater. Today Bio* **2020**, *8*, 100085.
[4] S. Guo, Q. Pan, M. B. Khamesee, *Microsyst. Technol.* **2008**, *14*, 307.
[5] X. Chen, M. Hoop, N. Shamsudhin, T. Huang, B. Özkale, Q. Li, E. Siringil, F. Mushtaq, L. Di Tizio, B. J. Nelson, *Adv. Mater.* **2017**, *29*, 1605458.
[6] A. Chałupniak, E. Morales-Narváez, A. Merkoçi, *Adv. Drug Delivery Rev.* **2015**, *95*, 104.
[7] C. C. J. Alcântara, F. C. Landers, S. Kim, C. De Marco, D. Ahmed, B. J. Nelson, S. Pané, *Nat. Commun.* **2020**, 11.
[8] H. Ceylan, I. C. Yasa, O. Yasa, A. F. Tabak, J. Giltinan, M. Sitti, *ACS Nano* **2019**, *13*, 3353.
[9] C. Hu, S. Pané, B. J. Nelson, *Annu. Rev. Control. Robot. Auton. Syst.* **2018**, *1*, 53.
[10] G. Go, A. Yoo, H.-W. Song, H.-K. Min, S. Zheng, K. T. Nguyen, S. Kim, B. Kang, A. Hong, C.-S. Kim, *ACS Nano* **2020**, *15*, 1059.
[11] S. Noh, S. Jeon, E. Kim, U. Oh, D. Park, S. H. Park, S. W. Kim, S. Pané, B. J. Nelson, J. Kim, *Small* **2022**, *18*, 2107888.
[12] S. R. Dabbagh, M. R. Sarabi, R. Rahbarghazi, E. Sokullu, A. K. Yetisen, S. Tasoglu, *Iscience* **2021**, *24*, 102012.
[13] S. R. Dabbagh, M. R. Sarabi, M. T. Birtek, S. Seyfi, M. Sitti, S. Tasoglu, *Nat. Commun.* **2022**, *13*, 5875.
[14] X.-H. Qin, A. Ovsianikov, J. Stampfl, R. Liska, *Bio. Nano. Materials* **2014**, *15*, 49.
[15] S. M. Oskui, G. Diamante, C. Liao, W. Shi, J. Gan, D. Schlenk, W. H. Grover, *Environ. Sci. Technol. Lett.* **2016**, *3*, 1.
[16] F. Rajabasadi, L. Schwarz, M. Medina-Sánchez, O. G. Schmidt, *Prog. Mater. Sci.* **2021**, *120*, 100808.
[17] J. Llacer-Wintle, A. Rivas-Dapena, X. Z. Chen, E. Pellicer, B. J. Nelson, J. Puigmartí-Luis, S. Pané, *Adv. Mater.* **2021**, *33*, 2102049.

[18] X. Wang, X. H. Qin, C. Hu, A. Terzopoulou, X. Z. Chen, T. Y. Huang, K. Maniura-Weber, S. Pané, B. J. Nelson, *Adv. Funct. Mater.* **2018**, *28*, 1804107.
[19] S. Muppalaneni, H. Omidian, J. Dev, *Drugs* **2013**, *2*, 1000112.
[20] A. Kumar, S. S. Han, *Int. J. Polym. Mater. Polym. Biomater.* **2017**, *66*, 159.
[21] M. A. Teixeira, M. T. P. Amorim, H. P. Felgueiras, *Polymers (Basel)* **2019**, *12*, 7.
[22] N. Ben Halima, *RSC Adv.* **2016**, *6*, 39823.
[23] S. Wu, M. Hua, Y. Alsaid, Y. Du, Y. Ma, Y. Zhao, C. Y. Lo, C. Wang, D. Wu, B. Yao, J. Strzalka, H. Zhou, X. Zhu, X. He, *Adv. Mater.* **2021**, *33*, 2007829.
[24] C. Mazzuca, L. Severini, F. Domenici, Y. Toumia, F. Mazzotta, L. Micheli, M. Titubante, B. Di Napoli, G. Paradossi, A. Palleschi, *Colloids Surf., B* **2020**, *188*, 110777.
[25] N. Vu Trung, N. Pham Thi, T. H. Nguyen, M. N. Nguyen, D. Tran Anh, T. Nguyen Trung, T. Tran Quang, H. Than Van, T. Tran Thi, *Polym. J.* **2022**, *54*, 335.
[26] R. Sadeghi, F. Jahani, *J. Phys. Chem. B* **2012**, *116*, 5234.
[27] M. Hua, S. Wu, Y. Ma, Y. Zhao, Z. Chen, I. Frenkel, J. Strzalka, H. Zhou, X. Zhu, X. He, *Nature* **2021**, *590*, 594.
[28] Y. Zhang, S. Furyk, D. E. Bergbreiter, P. S. Cremer, *J. Am. Chem. Soc.* **2005**, *127*, 14505.
[29] D. in Kim, H. Lee, S. hyun Kwon, H. Choi, S. Park, *Sensors Actuators, B Chem.* **2019**, *289*, 65.
[30] J. Liu, S. Yu, B. Xu, Z. Tian, H. Zhang, K. Liu, X. Shi, Z. Zhao, C. Liu, X. Lin, G. Huang, A. A. Solovev, J. Cui, T. Li, Y. Mei, *Appl. Mater. Today* **2021**, *25*, 101237.
[31] Z. Wang, D. Fu, D. Xie, S. Fu, J. Wu, S. Wang, F. Wang, Y. Ye, Y. Tu, F. Peng, *Adv. Funct. Mater.* **2021**, *31*, 2101648.
[32] C. de Marco, C. C. J. Alcântara, S. Kim, F. Briatico, A. Kadioglu, G. de Bernardis, X. Chen, C. Marano, B. J. Nelson, S. Pané, *Adv. Mater. Technol.* **2019**, *4*, 1900332.
[33] I. Bernardeschi, M. Ilyas, L. Beccai, *Adv. Intell. Syst.* **2021**, *3*, 2100051.
[34] P. Boonsuk, K. Kaewtatip, S. Chantarak, A. Kelarakis, C. Chaibundit, *J. Appl. Polym. Sci.* **2018**, *135*, 46406.
[35] L. Lartigue, D. Alloyeau, J. Kolosnjaj-Tabi, Y. Javed, P. Guardia, A. Riedinger, C. Péchoux, T. Pellegrino, C. Wilhelm, F. Gazeau, *ACS Nano* **2013**, *7*, 3939.
[36] M. Levy, N. Luciani, D. Alloyeau, D. Elgrabli, V. Deveaux, C. Pechoux, S. Chat, G. Wang, N. Vats, F. Gendron, C. Factor, S. Lotersztajn, A. Luciani, C. Wilhelm, F. Gazeau, *Biomaterials* **2011**, *32*, 3988.
[37] Y. Zhang, X. Li, Y. Zhang, J. Wei, W. Wang, C. Dong, Y. Xue, M. Liu, R. Pei, *New J. Chem.* **2021**, *45*, 7918.
[38] M. Hoop, A. S. Ribeiro, D. Rösch, P. Weinand, N. Mendes, F. Mushtaq, X. Z. Chen, Y. Shen, C. F. Pujante, J. Puigmartí-Luis, J. Paredes, B. J. Nelson, A. P. Pêgo, S. Pané, *Adv. Funct. Mater.* **2018**, *28*, 1705920.
[39] V. M. Kadiri, C. Bussi, A. W. Holle, K. Son, H. Kwon, G. Schütz, M. G. Gutierrez, P. Fischer, *Adv. Mater.* **2020**, *32*, 2001114.
[40] E. Chiellini, A. Corti, S. D'Antone, R. Solaro, *Prog. Polym. Sci.* **2003**, *28*, 963.
[41] D. C. Kong, M. H. Yang, X. S. Zhang, Z. C. Du, Q. Fu, X. Q. Gao, J. W. Gong, *Macromol. Mater. Eng.* **2021**, *306*, 2100536.
[42] Q. He, Y. Huang, S. Wang, *Adv. Funct. Mater.* **2018**, *28*, 1705069.
[43] B. E. B. Jensen, A. A. A. Smith, B. Fejerskov, A. Postma, P. Senn, E. Reimhult, M. Pla-Roca, L. Isa, D. S. Sutherland, B. Städler, A. N. Zelikin, *Langmuir* **2011**, *27*, 10216.
[44] S. Adepu, S. Ramakrishna, *Molecules* **2021**, *26*, 5905.
[45] S. Bashyal, C. Y. Shin, S. M. Hyun, S. W. Jang, S. Lee, *Pharmaceutics* **2020**, *12*, 270.
[46] M. Guo, Z. Yin, F. Chen, P. Lei, *Alzheimer's Res. Ther.* **2020**, *12*, 109.
[47] S. Tottori, L. Zhang, F. Qiu, K. K. Krawczyk, A. Franco-Obregõn, B. J. Nelson, *Adv. Mater.* **2012**, *24*, 811.